Sci. Bull. (2015) 60(17):1517–1526
DOI 10.1007/s11434-015-0876-y

www.scibull.com
www.springer.com/scp

Article

Engineering Sciences

Multi-objective hydraulic optimization and analysis in a minipump

Bin Duan · Minqing Luo · Chao Yuan · Xiaobing Luo

Received: 3 July 2015 / Accepted: 5 August 2015 / Published online: 22 August 2015

Abstract Minipump is widely used in microfluidics system, active cooling system, etc. But building a high efficiency minipump is still a challenging problem. In this paper, a systematic method was developed to design, characterize and optimize a particular mechanical minipump. The optimization work was conducted to cope with the conflict between pressure head and hydraulic efficiency by an improved back-propagation neural network (BPNN) with the non-dominated sorting genetic algorithm-II (NSGA-II). The improved BPNN was utilized to predicate hydraulic performance and, moreover, was modified to improve the prediction accuracy. The NSGA-II was processed for minipump multi-objective optimization which is dominated by four impeller dimensions. During hydraulic optimization, the processing feasibility was also taken into consideration. Experiments were conducted to validate the above optimization methods. It was proved that the optimized minipump was improved by about 24 % in pressure head and 4.75 % in hydraulic efficiency compared to the original designed prototype. Meanwhile, the sensitivity test was used to analyze the influence of the four impeller dimensions. It was found that the blade outlet angle β_2 and the impeller inlet diameter D_0 significantly influence the pressure head H and the hydraulic efficiency η, respectively. Detailed internal flow fields showed that the optimum model can relieve the impeller wake and improve both the pressure distribution and flow orientation.

Electronic supplementary material The online version of this article (doi:10.1007/s11434-015-0876-y) contains supplementary material, which is available to authorized users.

B. Duan · M. Luo · C. Yuan · X. Luo (✉)
School of Energy and Power Engineering, Huazhong University of Science and Technology, Wuhan 430074, China
e-mail: Luoxb@hust.edu.cn

Keywords Minipump · Optimization · Back-propagation neural network · Non-dominated sorting genetic algorithm-II

1 Introduction

Over the last decade, the microfluidic systems have been developing at an exponential rate and widely applied in chemical analysis [1], polymer chain reaction [2], microelectronics cooling [3] and other fields. The micropump is the essential actuation component in microfluidic systems. It can pump, control or otherwise manipulate small fluid volumes against backpressure through the system [4].

A variety of micro- or minipumps have been developed based on various principles [5–10]. Mostly, the motivation of the pump development focuses on the pumping realization to adapt with the microfluidic components, operation ambient, and moreover the micro processing method. The performance effectiveness analysis and optimization, by contrast, play second fiddle. Several numerical modeling and optimization designs were presented according to the pumping mechanism. Da Silva et al. [11] proposed a viscous pump with a cylindrical rotor set in the channel housing. By comparing sets of channel dimensions and the rotor eccentricity, the optimum model was obtained to maximize the mass flow rate per unit of shaft power consumption. Choi et al. [12] developed a dual rotating cylinders pump. By taking the advantage of the sequential metamodel-based optimization algorithm, the optimum design variables were automatically determined within the specific constraint; meanwhile, the relation between the objectives was revealed.

We proposed a mechanical centrifugal minipump with a 2 L/min flow rate, 90 kPa pressure head at 22,000 r/min

[13]. Figure 1 illustrates the components of the minipump. It generally consists of an impeller, a volute and a permanent magnet motor. Though this centrifugal minipump gets the similar form with the conventional pump, the hydraulic performance in conventional machine can be rarely referred to in minisize. In our previous work [13], it was demonstrated that the minipump equipped with open impeller could generate higher pressure head than that with the closed impeller while presenting a slightly efficiency drop. At the case of minisize, the leakage and disk friction of the closed impeller accounted for a large proportion in the overall power loss. Hence, to investigate the characteristics of geometry and flow in minisize is necessary.

In this paper, our study focuses on improving the hydraulic performance upon the open impeller model. This paper applied back-propagation neural network (BPNN) as a surrogate model to make prediction for the hydraulic performance, and non-dominated sorting genetic algorithm-II (NSGA-II) to optimize the objectives of pressure head and efficiency. Different from the existed works [14–17], to obtain a satisfied prediction accuracy overcoming inadequate training sample, this paper modified the standard BP network by combing with an enhanced simulated annealing (ESA) algorithm. The global sensitivity test was conducted to assess the influence of every decision variable upon the objective functions. Detailed operating curves and internal flow fields between the reference and optimum minipumps are analyzed.

2 Optimization statement

The overall optimization procedure can be generally described as follow: firstly, an original minipump is designed according to the partial emission pump theory. Secondly, the optimization space for four impeller variables is determined. After that, a training sample is established to construct the BPNN. Thirdly, the BPNN model is adopted instead of numerical calculation for objective prediction. Finally, with the obtained prediction model, the optimum minipump is selected by the NSGA-II.

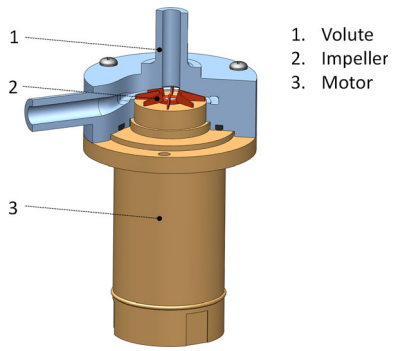

Fig. 1 (Color online) Components of the centrifugal minipump

2.1 Original design of minipump

The original reference minipump was designed to nominally generate a pressure head higher than 90 kPa under 2 L/min, 20,000 r/min. Through numerical simulation, the initial minipump model generates a pressure head of 99.56 kPa, and 46.98 % hydraulic efficiency at nominal operation conditions, which meet the given design objective. The detailed dimensions of the reference minipump will be given in the following.

2.2 Objective functions

Two objective functions are involved in this study including the pressure head H and the hydraulic efficiency of the impeller η, which are defined as

$$H = H_2 - H_1, \tag{1}$$

$$\eta = \frac{\rho g H Q}{P}, \tag{2}$$

where H, H_1, H_2, ρ, g, Q, and P represent the total head rise, inlet total pressure, outlet total pressure, density, gravity acceleration, volume flow rate and power, respectively.

2.3 Decision variables

Figure 2 illustrates the profile and design variables of the hydrodynamic components. The impeller design obeys the partial emission pump model; meanwhile, structure dimensions also shows high respect to processing consideration. Figure 2a shows the axial projection. The blade top and bottom edges are fixed by the tip clearances (x_1, x_2) which refer to the motor shaft axial displacement. The angle between the blade inlet edge and the hub γ (as shown in Fig. 2c) is defined as an 82° draft angle, which means the blade inlet diameter D_1 is subject to the inlet diameter D_0. As a result, the blade axonometric profile is dominated by the impeller inlet diameter D_0 and impeller outer diameter D_2. Figure 2b shows the plane projection. The impeller blades are 2-D arc curved. Thus, the vane spine line can be shaped by the blade inlet angle β_1 and blade outlet angle β_2. In addition, thickness is one of the manufacturing constraints. Therefore, the blade thickness distributions were frozen in optimization process. Finally, four design variables (Fig. 2) are employed as the decision parameters: impeller inlet diameter D_0, impeller outer diameter D_2, blade inlet angle β_1, blade outlet angle β_2.

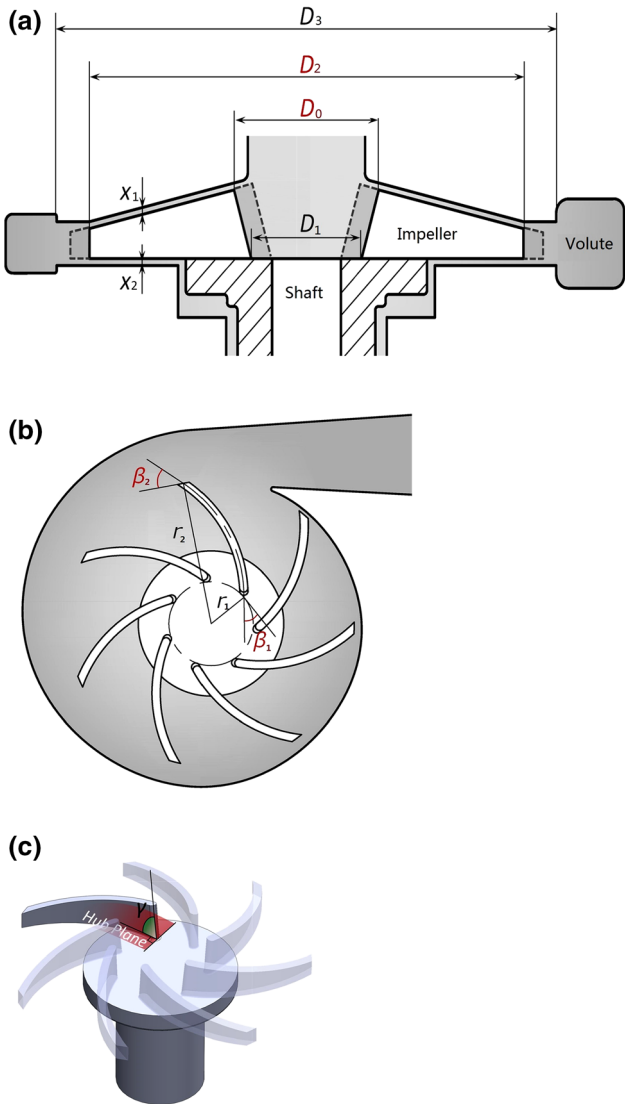

Fig. 2 (Color online) The profile and design variables of the hydrodynamic components. **a** Axial projection, **b** plane projection, **c** 3D impeller model and draft angle of inlet edge

Table 1 lists the variables design space based on traditional pump design theory and former design and experiment experiences. Evidently, the upper bound of D_2 is limited to the base circle diameter of the volute. The range of β_1 and β_2 are initially determined wider for parameter characterization; then, the variables space would be adjusted based on optimization results and sensitivity test in Sect. 4.

Table 1 Original minipump design parameters and design variables space

Decision variables	D_0 (mm)	D_2 (mm)	β_1 (°)	β_2 (°)
Reference model	4.4	14	25	60
Lower bound	2.8	12.8	19	25
Upper bound	5.8	14.2	49	70

As tabulated in Table S1 (online), a 40 points sample pool is established for neural network training. The sample points are selected by Latin hypercube sampling (LHS) [18] which is a typical stratified sampling. The principle is to divide the sample space into m mutually exclusive regions. Meanwhile, random samples from each region are taken based on each input variable's assigned distribution. The design space for each factor can be uniformly represented and also the variance could reduce significantly comparing with the random sampling [19].

The objective prediction of the sample is analyzed by solving the Reynolds-averaged Navier–Stokes equations (RANS) equations combined with the standard k–ε model and nonslip wall condition. The detailed numerical calculation process and validated the prediction accuracy were presented in our previous work [13]. The fluid domain is meshed with hybrid unstructured hexahedral and tetrahedral elements. To obtain high precise calculation based on the turbulence model, the overall value of Y^+ is less than 50 which is determined by the global Reynolds number approximately 315, 611 ($Re = \rho u_2 D_2/\mu$, where u_2 denotes the peripheral speed of the impeller, and the characteristic length refers to the impeller outlet diameter D_2). Before simulating the hydraulic performance of different impeller models, convergence study on grids is conducted with various numbers of grids. They are refined until the flow field changes less than 0.5 %. Finally, 465 and 2,197 grids are used in the simulation.

3 Objective prediction model

3.1 Application of simulated annealing in the topology design of BPNN

Once the training sample is established, a BPNN can be constructed as a surrogate model to make predictions for the objective functions. BPNN [20] is a multilayer feed-forward network which weights and biases are trained by the error back-propagation algorithm. This network is proved to approximate any nonlinear mapping. However, to guarantee the prediction accuracy, BPNN requires an adequate training sample which would lead to costly numerical computation. Otherwise, it may be trapped into local optimum ability and difficult to get satisfactory generalization. Therefore, one method is to leverage the advantages of global optimization algorithm to accelerate the evolving speed of neural network and improve the forecasting precision [21, 22].

To deal with the small sample learning problem, two measures are taken in this paper: (1) Introducing

generalization error as the termination criterion for the neural network; (2) Combining an enhanced simulated annealing algorithm (SA) [23] to modify the BPNN.

Here the generalization error [24] is typical to represent the prediction deviation of the network as the training sample is inadequate, and the detailed introduction is described in appendices. The SA is a global optimization algorithm, by means of "annealing temperature" t, the solution holds the probability: $P = \exp(-\Delta E/t)$ to escape from the current local optimum, where E is the generalization error.

The general concept of the present SA-BP structure is applying SA to globally search the optimum weights and biases sequence to reconstitute the BP network topology that meets the minimum generalization error. Figure 3 illustrates the SA-BP algorithm model procedure. The major steps are introduced as follows:

(1) *The weights and biases boundary establishment* The BP algorithm is applied for preliminary calculation to initialize the network. Then weights and biases sequences are extracted to estimate the initial boundary. The purpose is to narrow the searching range of SA and improve calculating efficiency. The boundary is flexible in the following steps.

(2) *SA searching* Performing the iteration process of "generating new solution—judging—accepting or rejecting" to search for the weights and biases optimum that minimize the generalization error. Adjust the weights and biases boundary when the optimum approaches the limit.

(3) *BP reconstitution* Updating the BP network and then verifying the feasibility of the SA-BP structure when the generalization error stabilizes.

Finally, a BP neural network with a hidden layer and five neuron nodes is applied to establish the performance-forecasting model for the minipump. After calculating, the generalization error of pressure head and efficiency are 3.4 %, 0.7 %, respectively. Furthermore, average relative

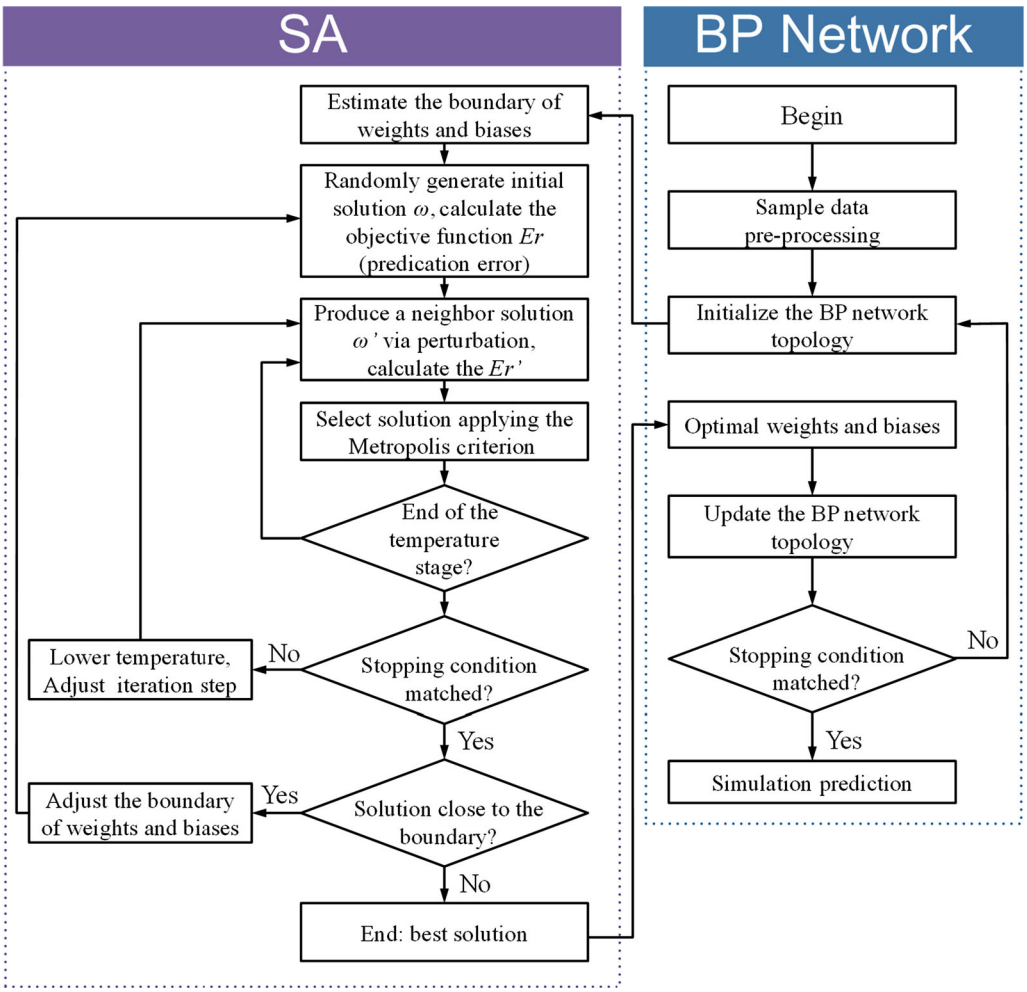

Fig. 3 (Color online) The procedure of the SA-BP algorithm model

variance *ARV*, absolute fraction of variance R^2 and root mean squared error *RMSE* are introduced to measure the prediction precision which are defined as follows:

$$ARV = \frac{\sum_{i=1}^{N}[x(i) - \hat{x}(i)]^2}{\sum_{i=1}^{N}[x(i) - \bar{x}(i)]^2}, \quad (3)$$

$$R^2 = 1 - \left(\frac{\sum_{i=1}^{N}[x(i) - \hat{x}(i)]^2}{\sum_{i=1}^{N}\hat{x}(i)^2}\right), \quad (4)$$

$$RMSE = \left(1/N\sum_{i=1}^{N}[x(i) - \hat{x}(i)]^2\right)^{1/2}, \quad (5)$$

where $x(i)$ is the target value, $\hat{x}(i)$ is the prediction output. Table 2 lists the statistical results of two BP networks. It is observed that SA can significantly improve the BP generalization performance, in particular the objective efficiency. The statistical results present the superiority of SA-BP structure considering small sample training. Hence, the SA-BP can be utilized as a surrogate model for the pressure head and efficiency optimization in NSGA.

4 Impeller optimization

This paper utilizes the NSGA-II to cope with the confliction of the pressure head and the efficiency optimums. The NSGA-II developed by Deb is the derivation of genetic algorithm (GA) [25] that comprise of sorting, crossover and mutation. The gut of NSGA-II is the non-dominated sorting with the introduction of crowding distance as the fitness. The principle can be described as follows: in each generation, the population is sorted into several fronts. The first front known as Pareto front is completely non-dominant set in the current population, while the subsequent front is dominated by the individuals in the first front only and the rest of the fronts go so on. Meanwhile, the individual in each front is not dominated by any other one. The crowding distance refers to surrounding individual density in the current front calculated by taking the average distance of the two points on both side of the individual along each objective. The individual with lower front rank or larger crowding distance (same front rank) gets large possibility to offspring. In this work, the gene is real-coded to shorten coding length and eliminate the error generated during encoding and decoding. The parameters in the algorithm are given as follows: population size, 100; generations, 600; crossover probability, 0.9; mutation probability, 0.1 and no further augment on population size.

Besides, the minimum blade pitch is the key limitation to the mold processing and cannot be narrower than 0.5 mm. Hence, this constraint is also embedded into NSGA for individual screening. The detailed geometrical formulation is introduced in the Electronic supplementary material.

Table 2 Statistical results of two BP networks

	Generalization error (%)	*ARV*	R^2	*RMSE*
Pressure head				
BP	4.4	0.26	0.9970	0.0537
SA-BP	3.4	0.12	0.9992	0.0234
Efficiency				
BP	2.1	0.921	0.9994	0.0120
SA-BP	0.7	0.156	0.9999	0.0049

4.1 Pareto-optimal frontier

Figure 4 shows the Pareto-optimal frontier (POF) of the NSGA with the SA-BP model. The top axis refers to efficiency value, and the right axis is pressure head. The bottom and left axes refer to the corresponding nondimensionalized value. Euclidian non-dimensionalization is utilized to normalize the objective functions space for the decision-making algorithm in Sect. 4.3. The nondimensionalized objective function is defined as,

$$P(i,j) = V(i,j) \Big/ \left(\sum_{i=1}^{N} V(i,j)^2\right)^{1/2}, \quad (6)$$

where i refers to the individual index in the POF, j refers to the objective function index, and $V(i, j)$ refers to the objective function value in the POF.

In order to fully analyze the geometric and hydrodynamic characteristic in the Pareto-optimal frontier, the individuals in the POF are decomposed into 4 clusters utilizing hierarchical clustering method. The clustering principle bases on the nearest distance from the weighted center of mass (as highlighted in Fig. 4). Table S2 (online)

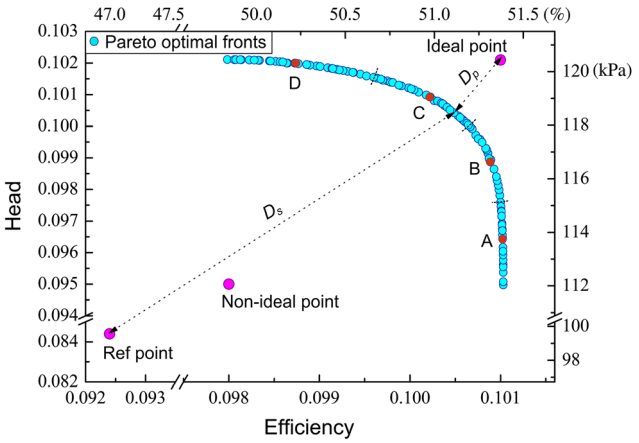

Fig. 4 (Color online) Pareto-optimal frontier through SA-BP

compares the POF solutions of the four typical centers with the corresponding numerical calculations. The maximum deviations of the SA-BP predictions from the relative RANS analysis are 1.98 % and 2.68 %, respectively, for the pressure head H and the hydraulic efficiency η, demonstrating the accuracy of the optimization method.

Table S3 lists the extreme values of the design variables and objective functions in the Pareto-optimal frontier and each cluster. The POF solutions show a large margin than the original reference minipump with 20.89 kPa and 4.41 % increase in H and η, respectively. It is notable that among the overall POF space, the impeller inlet diameter D_0 varies within 34 % of the decision variables space and gathers near the lower bound, and the impeller outlet diameter D_2 gathers in 33 % of the decision variables space near the upper bound, while the blade inlet angle β_1 and the blade outlet angle β_2 are fixed near the upper bound. In clusters A, B, the pressure head improves 5.6 kPa at the cost of 0.16 % hydraulic efficiency drop. In cluster D, a 0.61 kPa drop in pressure head can increase 0.8 % in hydraulic efficiency (accounts for nearly 50 % in the POF range).

Graphically, the box charts of D_0, D_2 in each cluster are illustrated in Fig. 5 to reveal the variability of the decision variables. It is observed that both of the design variables show an increasing trend to improve the pressure head. As to the cluster A, the D_0 lies near the minimum with little variability which reflects that in cluster A, the objective variables are sensitive to D_0. Therefore, the steep increase in pressure head as shown in Fig. 5 is mainly subject to the D_2. Likewise, the objective variables in cluster D are sensitive to D_2, and the efficiency is influenced by D_0.

4.2 Decision variables characterization

In order to assess the influence of every decision variable upon the objective functions (known as sensitivity), and provide references for future parameter range determination, the Sobol' method is applied for global sensitivity test [26]. This method is a Monte Carlo analysis based on variance to reflect the output uncertainty according to different decision variables. It can not only measure the independent variable effect on the objective function, which refers to the fraction of the total output variance contributed by a particular variable i in isolation, the so-called first-order global sensitivity (S_i), but also calculate the total global sensitivity (TS_i) which refers to the sum of all the sensitivities involving the particular variable i, hence reflects the interactions between the decision variables. The definitions are given as,

$$S_i = \frac{D_i}{D}, \tag{7}$$

$$\mathrm{TS}_i = \frac{\sum_{j=1}^{n} D_{i1\cdots ij}}{D}. \tag{8}$$

Figure 6 shows the first-order and total sensitivities of the decision variables. The pressure head H is mainly contributed by the blade outlet angle β_2 and moderately by the impeller outer diameter D_2. Meanwhile, the influence of the other parameters is negligible, indicating that they can keep constant under the case of single object optimization for pressure head. In addition, the first-order sensitivities are parallel to the according total sensitivities, suggesting that the decision variables are independent. For hydraulic efficiency, D_0 and β_1 have considerable influence, and the interactions involving D_0 are notable.

Hence, combining the results of the POF and sensitivity test, suggestion could be given that, the optimization range of D_0 and β_2 should be narrow down to further improve the prediction precision considering the significant sensitivity at the present variable space. Oppositely, the variable space of β_1 could be broadened properly. Moreover, as β_1 and β_2 reach the upper bound in POF, the relevant upper bound should be raised for the future optimization.

4.3 Optimum minipump selection

The final optimum minipump should be determined to typically integrate both prominent pressure head and efficiency performance. In Fig. 4, we can see that every individual in

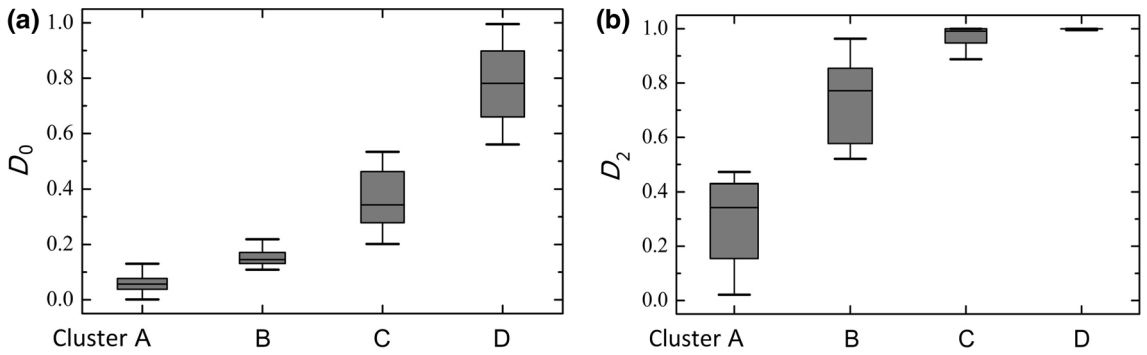

Fig. 5 Box chart of D_0 (**a**), D_2 (**b**) in each cluster

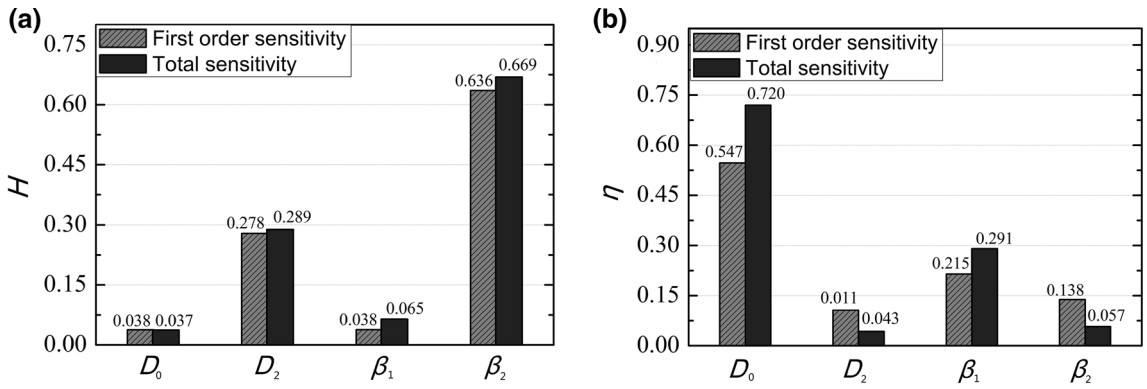

Fig. 6 The first-order and total sensitivity of the decision variables to pressure head (**a**), hydraulic efficiency (**b**)

the POF is superior to the original reference, and the arbitrary choice of one individual in the nondominated set over the other is biased and unacceptable with respect to all objectives. One common approach for decision making is to compare the scalar of the objective vectors by designating corresponding weights to the objectives. The obtained solution largely depends on engineering experiences and weight factor of each objective. In literature [27], the best two-object optimization solution is located at the vertical point from the ideal point to the POF hence the closest distance of both, representing the best possible values for objectives. The ideal point illustrated in Fig. 4 represents the optimum objective values in the POF, and the non-ideal point goes to minimum. This paper employs technique for order preference by similarity to ideal solution (TOPSIS) method (detailed in Ref. [28]) for decision making from the POF results. Nevertheless, the D_S introduced here represents the distance to the reference point rather than to the non-ideal point, as defined

$$D_S = \left(\sum_{j=1}^{n} [P(j) - P_R(j)]^2 \right)^{1/2}, \quad (9)$$

where n refers to the objective dimension, j refers to the objective index, $P(j)$ refers to the objective function in the POF, $P_R(j)$ refers to the objective function of the original reference. The objective function is nondimensionalized (Eq. (6)).

Hence the criterion B is defined as follows,

$$B = \frac{D_S}{D_P + D_S}, \quad (10)$$

where the D_p represents the distance to the ideal point as shown in Fig. 4.

The maximum criterion B is determined as the typical solution implies that it contains the considerations to widen the difference from the original reference and to approach the ideal situation. Finally, the TOPSIS point with the criterion B of 0.931 is selected as the optimum model. Table S2 provides the detail design and objective values. It is noteworthy that this selection method maybe changed or unacceptable in other situation.

5 Model validation

To validate the optimization process introduced above, we manufactured the optimum minipump prototype. The objective hydraulic performance was measured through the minipump testing loop [13]. The pressure head is measured via the inlet and outlet pressure ports using differential pressure transducers (Yokogawa, EJA110A), and the volumetric flow rate is measured with an electromagnetic flow-meter (Yokogawa, AXF005G). The accuracy of the pressure and flow sensors are less than or equal to 6.5 % kPa and 4.14 % L/min, respectively. A temperature control unit is set in the reservoir to ensure a stable system liquid temperature. Meanwhile, numerical simulation was implemented based on computational fluid dynamics (CFD) to compare the flow field properties.

5.1 External characteristic

Figure 7 shows the fabricated minipump prototype. The entire system uses stainless steel and weighs 166 g. The overall length is 84 mm including the electrical terminal. The brushless DC motor is driven by a 28 V controller and can rotate from 10,000 to 25,000 r/min.

Figure 8 presents the H–Q results comparison between the reference and TOPSIS model at 3 rotational speeds. It is noted that the deviation between numerical prediction and experiment result increases as the flow rate decreasing. The reason is observed that the minipump operating conditions deteriorates because of the impeller axial play getting intense when the flow rate decreases. The highest deviation under 400 mL/min is found to be 6.5 % at 20,000 r/min for the reference

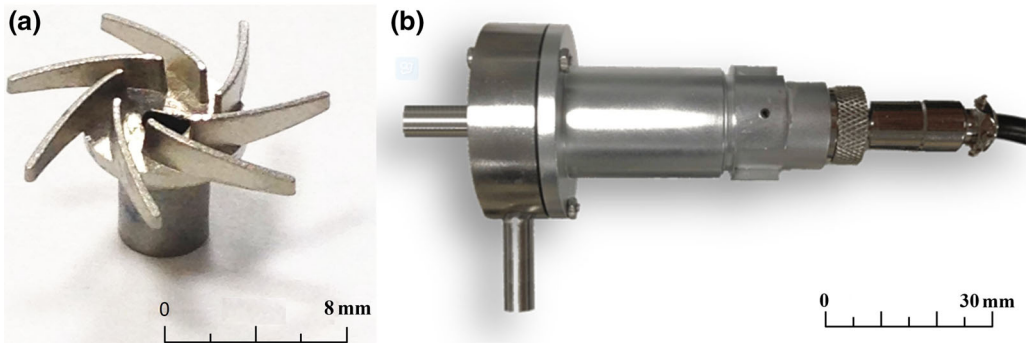

Fig. 7 (Color online) The minipump prototype. **a** The fabricated impeller, **b** the minipump assembly

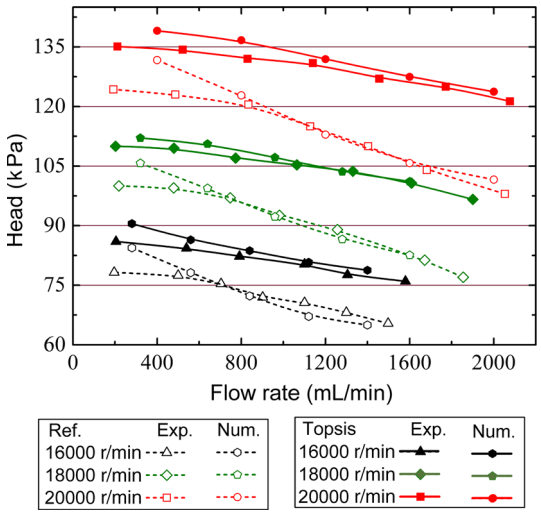

Fig. 8 (Color online) *H–Q* results comparison between the reference and TOPSIS model

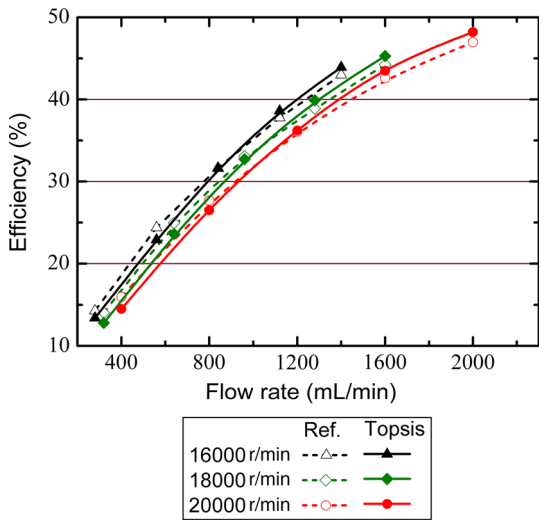

Fig. 9 (Color online) *η-Q* results comparison between the reference and TOPSIS model

model. When larger than 600 mL/min, the highest and average deviation for both models are 3.9 % and 2.0 %, respectively, demonstrating that the numerical simulation has a high accuracy to predict the minipump flow field. The TOPSIS minipump presents gentle operating curves comparing with the reference one. Significantly, the TOPSIS model generates a much higher pressure head than the reference model over the full range of flow rate at 3 rotational speeds. The pressure head deviation increases as the flow rate increasing and reaches 24.2 % at 2,050 mL/min, 20,000 r/min.

Figure 9 shows the overall efficiency comparison between the reference and TOPSIS model. The hydraulic efficiency improves about 1.5 % as the rotational speed drops 2,000 r/min. The best efficiency point delays at 2 L/min for the both models. It is observed that the efficiency of the reference model is higher than the TOPSIS at small flow rate, while the situation goes to the contrary side with the increase in flow rate. Besides, the efficiency difference is minor over the full range of flow rate at 3 rotational speeds. The highest deviation is relatively 4.75 % at 2,000 mL/min, 20,000 r/min, reflecting that the optimum selection strategy tend to significantly improve the pressure head compared to efficiency. According to the POF solutions, the hydraulic efficiency can increase relatively 8.8 % at the expense of sacrificing the head pressure (For example, see point *A* in Fig. 4).

5.2 CFD flow field

Figure 10 shows the static pressure contours at the plane located in the middle height of the minipump for the nominal condition. It is observed that the TOPSIS model can smoothen the contour curves along the impeller passage comparing to the reference. Meanwhile, the low pressure region in the latter caused by the impeller wake messes up the pressure distribution in the volute, especially near the laryngeal. Those situations are suppressed in TOPSIS impeller. Figure 11 shows the static pressure contour slices at the central *X–Y* plane of the minipump for

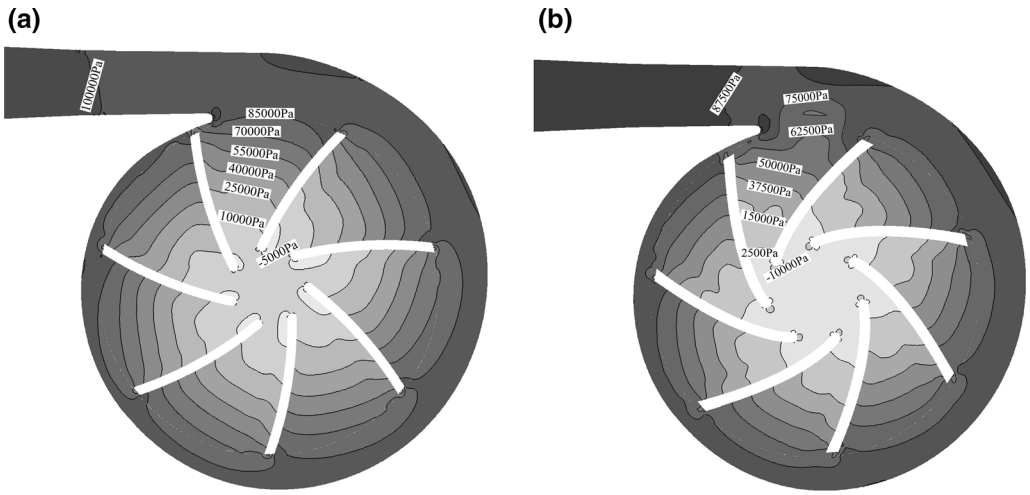

Fig. 10 Static pressure contours (Unit: Pa) at the plane located in the middle height of the minipump for the nominal condition. **a** TOPSIS model, **b** reference model

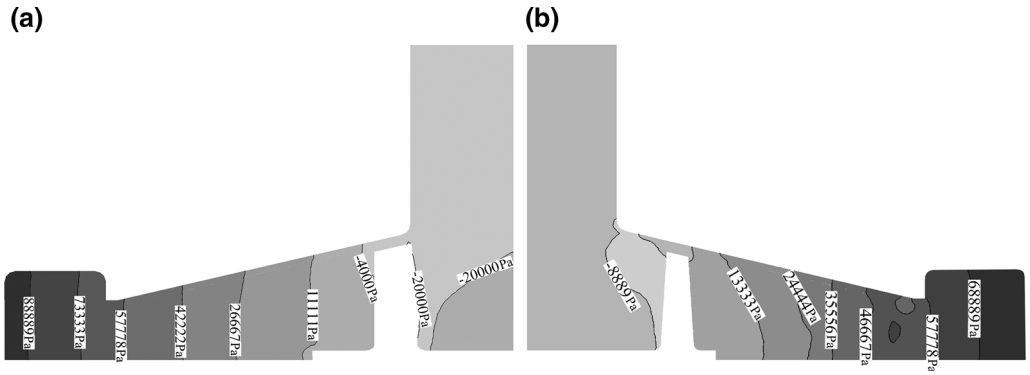

Fig. 11 Static pressure contour (Unit: Pa) slices at the central *X*–*Y* plane of the minipump for the nominal condition. **a** TOPSIS model, **b** reference model

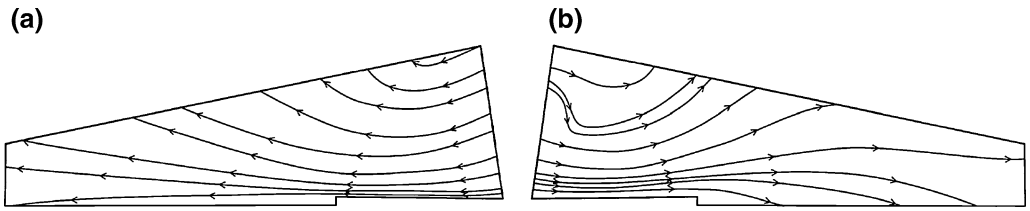

Fig. 12 Streamline paths at the pressure surface of the impeller for the nominal condition. **a** TOPSIS model, **b** reference model

the nominal condition. Similarly, the low pressure region completely clogs the impeller inlet which would yield the flow stream. Near the impeller passage outlet occur the uneven pressure spots further aggravating the turbulence intensity. On the contrary, the TOPSIS impeller generates a smooth and steady pressure filed from the inlet to the volute. The pressure distribution is more regular as the contour curves going parallel to the blade section. Figure 12 illustrates the streamline paths at the pressure surface of the impeller for the nominal condition. As expected, the streamlines are badly oriented in the reference minipump near the impeller inlet. The large recirculation zone spotted in the reference model is improved in the TOPSIS impeller.

Thus it is proved that the TOPSIS minipump can both smooth the pressure distribution and improve the flow orientation, and these are the main reasons to raise the hydraulic efficiency.

6 Conclusions

The current work presents a systematic method to design, characteristic and optimize the mechanical minipump. We introduced the generalization error into the neural network to improve the generalization performance at the case of small sample training. Compared to the standard BP network, the statistical results show that SA-BP network can significantly improve the prediction accuracy, particularly for the objective efficiency. The optimized minipump was proved to improve 24 % in pressure head and 4.75 % in hydraulic efficiency.

NSGA and sensitivity test give an overall insight into the decision variables characteristic. Referring to the POF generated by NSGA, the high pressure head situation presents an impeller profile with larger D_0 and D_2. While at the high efficiency condition, the pressure head is mainly influenced by D_2. The sensitivity test shows that the pressure head H is mainly contributed by β_2 and moderately by D_2. While for hydraulic efficiency, D_0 and β_1 have considerable influence, and the interactions involving D_0 are notable. From the CFD analysis, the optimum model can relieve the impeller wake and improve both the pressure distribution and flow orientation.

Conflict of interest The authors declare that they have no conflict of interest.

References

1. Fan X, White IM (2011) Optofluidic microsystems for chemical and biological analysis. Nat Photonics 5:591–597
2. Hua Z, Rouse JL, Eckhardt AE et al (2010) Multiplexed real-time polymerase chain reaction on a digital microfluidic platform. Anal Chem 82:2310–2316
3. Dang B, Bakir MS, Sekar DC et al (2010) Integrated microfluidic cooling and interconnects for 2D and 3D chips. IEEE Trans Adv Packag 33:79–87
4. Laser DJ, Santiago JG (2004) A review of micropumps. J Micromech Microeng 14:R35–R64
5. Nguyen NT, Huang X, Chuan TK (2002) MEMS-micropumps: a review. J Fluid Eng 124:384–392
6. Ahn CH, Allen MG (1995) Fluid micropumps based on rotary magnetic actuators. In: Proceedings of 1995 IEEE micro electro mechanical systems workshop (MEMS'95), Amsterdam, Netherlands, pp 408–412
7. Blanchard D, Ligrani P, Gale B (2005) Performance and development of a miniature rotary shaft pump. J Fluid Eng 127:752–760
8. Li Z, Wang M, Tan L (2002) Experimental investigation on phase transformation type micropump. Chin Sci Bull 47:519–523
9. Zhang J, Leng X, Zhao C (2014) A spiral-tube-type valveless piezoelectric pump with gyroscopic effect. Chin Sci Bull 59:1885–1889
10. Yu H, Yu J, Ma CF (2010) Design, fabrication and experimental research for an electrohydrodynamic micropump. Sci China Tech Sci 53:2839–2845
11. Da Silva AK, Kobayashi MH, Coimbra CFM (2007) Optimal design of non-Newtonian, micro-scale viscous pumps for biomedical devices. Biotechnol Bioeng 96:37–47
12. Choi HI, Lee Y, Choi DH et al (2010) Design optimization of a viscous micropump with two rotating cylinders for maximizing efficiency. Struct Multidiscipl Optim 40:537–548
13. Duan B, Guo TH, Luo MQ et al (2014) A mechanical micropump for electronic cooling. In: The intersociety conference on thermal and thermomechanical phenomena in electronic systems (IEEE ITHERM), Orlando, USA, pp 1038–1042
14. Zhang J, Zhu H, Yang C et al (2011) Multi-objective shape optimization of helico-axial multiphase pump impeller based on NSGA-II and ANN. Energy Conv Manag 52:538–546
15. Husain A, Kim KY (2010) Enhanced multi-objective optimization of a microchannel heat sink through evolutionary algorithm coupled with multiple surrogate models. Appl Therm Eng 30:1683–1691
16. Wang TG, Wang L, Zhong W et al (2012) Large-scale wind turbine blade design and aerodynamic analysis. Chin Sci Bull 57:466–472
17. Bing H, Cao SL (2013) Multi-parameter optimization design, numerical simulation and performance test of mixed-flow pump impeller. Sci China Tech Sci 56:2194–2206
18. McKay MD, Conover WJ, Beckman RJ (1979) A comparison of three methods for selecting values of input variables in the analysis of output from a computer code. Technometrics 21:239–245
19. Florian A (1992) An efficient sampling scheme: updated latin hypercube sampling. Probab Eng Mech 7:123–130
20. Rumelhart DE, Hinton GE, Williams RJ (1986) Learning internal representations by error propagation. MIT Press, Cambridge, pp 318–362
21. Huang CR, Tang JL, Liu YJ (2011) A new face detection method with GA-BP neural network. (WiCOM). In: 7th international conference on wireless communications, networking and mobile computing, pp 1–4
22. Liu YP, Wu MG, Qian JX (2007) Predicting coal ash fusion temperature based on its chemical composition using ACO-BP neural network. Thermochim Acta 454:64–68
23. Siarry P, Berthiau G, Durdin F et al (1997) Enhanced simulated annealing for globally minimizing functions of many-continuous variables. ACM Trans Math Softw 23:209–228
24. Queipo NV, Haftka RT, Shyy W et al (2005) Surrogate-based analysis and optimization. Prog Aerosp Sci 41:1–28
25. Deb K, Pratap A, Agarwal S et al (2002) A fast and elitist multiobjective genetic algorithm: NSGA-II. IEEE Trans Evol Comput 6:182–197
26. Sobol' IM (2001) Global sensitivity indices for nonlinear mathematical models and their Monte Carlo estimates. Math Comput Simul 55:271–280
27. Sayyaadi H, Babaelahi M (2011) Multi-objective optimization of a joule cycle for re-liquefaction of the Liquefied Natural Gas. Appl Energy 88:3012–3021
28. Sayyaadi H, Mehrabipour R (2012) Efficiency enhancement of a gas turbine cycle using an optimized tubular recuperative heat exchanger. Energy 38:362–375

Copyright Information

For Authors

As soon as an article is accepted for publication, authors will be requested to assign copyright of the article (or to grant exclusive publication and dissemination rights) to Science China Press and Springer. This will ensure the widest possible protection and dissemination of information under copyright laws.

More information about copyright regulations for this journal is available at www.springer.com/11434.

For Readers

While the advice and information in this journal is believed to be true and accurate at the date of its publication, neither the authors, the editors, nor the publishers can accept any legal responsibility for any errors or omissions that may have been made. The publishers make no warranty, express or implied, with respect to the material contained herein.

All articles published in this journal are protected by copyright, which covers the exclusive rights to reproduce and distribute the article (e.g., as offprints), as well as all translation rights. No material published in this journal may be reproduced photographically or stored on microfilm, in electronic data bases, on video disks, etc., without first obtaining written permission from the publisher (respectively the copyright owner if other than Springer). The use of general descriptive names, trade names, trademarks, etc., in this publication, even if not specifically identified, does not imply that these names are not protected by the relevant laws and regulations.

Springer has partnered with Copyright Clearance Center's RightsLink service to offer a variety of options for reusing Springer content. For permission to reuse our content please locate the material that you wish to use on link.springer.com or on springerimages.com and click on the permissions link or go to copyright.com, then enter the title of the publication that you wish to use. For assistance in placing a permission request, Copyright Clearance Center can be connected directly via phone: +1-855-239-3415, fax: +1-978-646-8600, or e-mail: info@copyright.com.

Abstracted/indexed in
Science Citation Index, Chemical Abstracts, SCOPUS, Google Scholar, Inspec, Academic Search Alumni Edition, Academic Search Complete, Academic Search Elite, Academic Search Premier, ASFA 1: Biological Sciences and Living Resources, ASFA 2: Ocean Technology, Policy and Non-Living Resources, Biological Sciences, Biological Abstracts, BIOSIS Previews, CAB Abstracts, Current Contents/Physical, Chemical and Earth Sciences, Current Mathematical Publications, Digital Mathematics Registry, EMBio, Environmental Engineering Abstracts, Environmental Sciences and Pollution Management, Mathematical Reviews, MathSciNet, Meteorological and Geoastrophysical Abstracts, Pollution Abstracts, Water Resources Abstracts, Zentralblatt MATH, Zoological Record.

Science Bulletin 科学通报 (英文版) Vol. 60 No. 17 September 15, 2015 (Semi-monthly)

Supervised by Chinese Academy of Sciences
Sponsored by Chinese Academy of Sciences and National Natural Science Foundation of China
Published by Science China Press and Springer-Verlag Berlin Heidelberg
Subscriptions
China Science China Press, 16 Donghuangchenggen North Street, Beijing 100717, China
Email: sales@scichina.org Fax: 86-10-64016350
The Americas (North, South, Central America and the Caribbean) Springer Journal Fulfillment, 233 Spring Street, New York, NY, 10013-1578, USA
Tel. 800-SPRINGER (777-4643); 212-460-1500 (outside North America) journals-ny@springer.com; servicio-ny@springer.com (Central and South America)
Outside the Americas Springer Customer Service Center GmbH, Haberstr. 7, 69126 Heidelberg, Germany
Tel.: +49-6221-345-4303 subscriptions@springer.com
Printed by Beijing Artownprinting Co., Ltd., Chuangyeyuan Road, Taihu Town, Tongzhou District, Beijing 101116, China
Edited by Editorial Board of Science Bulletin, 16 Donghuangchenggen North Street, Beijing 100717, China
Editor-in-Chief Xiao-Ya Chen

CN 10-1298/N ISSN (Print) 2095-9273 ISSN (Online) 2095-9281
广告经营许可证: 京东工商广字第0429号
邮发代号: 80-214 (英)
国内每期定价: 180元

http://www.scibull.com

Science Bulletin

Articles | Reviews | Letters | News & Views | Research Highlights | Comments | Correspondences | etc.

High impact—a semi-monthly multidisciplinary journal co-sponsored by the Chinese Academy of Sciences and the National Natural Science Foundation of China

Broad coverage—reports on significant advances across a broad range of natural sciences and engineering fields around the globe

Rapid publication—a fast-paced platform for cutting-edge research findings, insightful reviews and news, and discussions of upcoming trends relevant to science and scientists

- **Indexed by SCI, CA, etc.**
- **Online First Publication**
- **Open Choice**

ISSN 2095-9273

9 772095 927159

《中国科学》杂志社 SCIENCE CHINA PRESS

Springer